catalysts

MDPI

*Article*

# UV-Activated and $Fe^{2+}$-Catalyzed $H_2O_2$ for the Treatment of Dye-Contaminated Water: Kinetics, Mechanism and Toxicity Investigations

**Wisal Ahmad [1], Roman Shah [1], Hameed Ul Haq [1], Dilaram Khan [1], Shahab Khan [2], Abdulaziz Al-Anazi [3], Javed Ali Khan [1,*], Nusrat Rezwana Binte Razzak [4] and Changseok Han [5,6,*]**

[1] Department of Chemistry, Abdul Wali Khan University Mardan, Mardan 23200, Pakistan; kwisal561@gmail.com (W.A.); romanshah2059@gmail.com (R.S.); ulhaqsamarbagh@gmail.com (H.U.H.); khandilaram63@gmail.com (D.K.)
[2] Department of Chemistry, University of Science and Technology, Bannu 28100, Pakistan; shahabsikandry74@gmail.com
[3] Department of Chemical Engineering, College of Engineering, King Saud University, P.O. Box 800, Riyadh 11421, Saudi Arabia; aalanazi15@ksu.edu.sa
[4] School of Engineering, Deakin University, Geelong, VIC 3216, Australia; nbinterazzak@deakin.edu.au
[5] Program in Environmental and Polymer Engineering, Graduate School of Inha University, 100 Inha-ro, Michuhol-gu, Incheon 22212, Republic of Korea
[6] Department of Environmental Engineering, Inha University, 100 Inha-ro, Michuhol-gu, Incheon 22212, Republic of Korea
* Correspondence: javedkhan@awkum.edu.pk or khanjaved2381@gmail.com (J.A.K.); hanck@inha.ac.kr (C.H.); Tel.: +92-937-929122 (C.H.); Fax: +92-937-542189 (C.H.)

**Abstract:** This study investigated the removal of methylene blue (MB) by different UV, UV-catalyzed $H_2O_2$ (UV/$H_2O_2$) and UV-and-iron-catalyzed $H_2O_2$ (UV/$H_2O_2$/$Fe^{2+}$)-based advanced oxidation processes. At pH 6.0, the removal of MB (15 mg/L) was found to be 6.31% at 60 min for UV only. However, the combination of $H_2O_2$ (5 mM) with UV greatly enhanced the removal efficiency as 96.44% degradation of MB was found in the UV/$H_2O_2$ process at 60 min. Furthermore, the UV/$H_2O_2$/$Fe^{2+}$ process was observed to be even more efficient than UV/$H_2O_2$, achieving 99.11% MB degradation at 30 min of treatment under the experimental conditions of $[MB]_0$ = 15 mg/L, $[H_2O_2]_0$ = 2 mM, $[Fe^{2+}]_0$ = 0.5 mg/L, and $pH_0$ = 3.0. Furthermore, the removal of TOC was found to be 59 and 71% for UV/$H_2O_2$ and UV/$H_2O_2$/$Fe^{2+}$, respectively. The pH did not change the efficiency of the UV/$H_2O_2$ process significantly; however, it greatly affected the efficiency of the UV/$H_2O_2$/$Fe^{2+}$ system. The results demonstrate that both UV/$H_2O_2$ and UV/$H_2O_2$/$Fe^{2+}$ could be used for the effective degradation and mineralization of MB.

**Keywords:** UV/$H_2O_2$; photo-Fenton; methylene blue; degradation; mechanism; water treatment



**Citation:** Ahmad, W.; Shah, R.; Haq, H.U.; Khan, D.; Khan, S.; Al-Anazi, A.; Khan, J.A.; Binte Razzak, N.R.; Han, C. UV-Activated and $Fe^{2+}$-Catalyzed $H_2O_2$ for the Treatment of Dye-Contaminated Water: Kinetics, Mechanism and Toxicity Investigations. *Catalysts* **2024**, *14*, 906. https://doi.org/10.3390/catal14120906

Academic Editors: Detlef W. Bahnemann and Yaron Paz

Received: 11 November 2024
Revised: 27 November 2024
Accepted: 4 December 2024
Published: 9 December 2024



## 1. Introduction

Unquestionably, water is a priceless natural resource that is essential for the maintenance of life. However, the world is facing the issue of restricted access to clean drinking water due to water contamination. When environmental stressors in the form of chemicals are introduced to water at concentrations beyond the maximum allowable level, pollution of the water results. Water contamination or pollution is due to the presence of various organic (dyes, hydrocarbons, pesticides, herbicides, phenols, fertilizers, biphenyls, oils, greases, proteins, carbohydrates, pharmaceuticals and so on) and inorganic chemicals (heavy metals and anions), as well as minerals from industry, agriculture and household sources [1]. One of the main causes of surface and groundwater contamination is industrial effluents. Due to rising urbanization and globalization, there is a rise in the demand for goods produced with colors and heavy metals [2]. Pigments and dyes are often used as

colorants in the food, textile and pharmaceutical sectors [3,4]. It is important to note that some of these dyes are carcinogenic and mutagenic **[5]**. The dyeing industries, which rely on synthetic pigments, have expanded globally, producing around 8105 tons of synthetic dyes annually [6]. The textile sector comprises approximately 75% of the worldwide market for dyestuffs. There are about ten thousand distinct types of dyes used to color and/or print various forms of cloth [7]. However, some of the dyes do not adhere effectively to the fabric or food; hence, the contamination of water results from the release of such industrial wastes [8]. Color is one of the simplest pollutants to detect with the naked eye. Since dyes are toxic, their removal from industrial effluents is necessary before their discharge into water bodies [9]. Aquatic species suffer from decreased amounts of dissolved oxygen due to the elevated chemical oxygen demand (COD) caused by dye contamination and other toxicity-related effects. These wastes, discharged by these industries, mostly contain synthetic colors, which hinder the photosynthetic processes of aquatic organisms due to the reduced penetration of sunlight into water bodies, thereby increasing the biochemical oxygen demand (BOD), and they have a detrimental impact on the food sources of aquatic organisms [10]. In addition to interfering with plant photosynthetic processes, the release of synthetic colors renders water unsuitable and undesirable on an aesthetic level [11]. Environmentalists and eco-toxicologists have already conducted research that has proven the carcinogenic effects on humans [12].

Methylene blue (3,7-is (dimethylamino) phenothiazine chloride tetra methylthionine chloride) is one of the most commonly used dyes in the textile industry [13,14]. It is used in the dyeing of silk, wool, paper and cotton [15–18]. It is released into natural water resources in high amounts by the textile industry, which is very harmful to animal and human health **[19]**. Due to its high toxicity, MB dye poses a risk to human health above certain concentrations [20]. Because of the toxicity of MB, its carcinogenic nature and its resistance to biodegradation, it poses a major risk to the health of humans and adversely affects ecosystems [21,22]. Several diseases, such as blindness and respiratory, mental and digestive disorders, are caused by wastewater containing MB [23]. Moreover, other diseases, such as increasing heartbeats, the death of new cells, eye and skin diseases, nausea and diarrhea, can also be caused by contaminated water containing MB [24,25]. Therefore, it is considered an industrial waste and hence should be removed from water bodies. Numerous techniques have been suggested for the treatment of wastewater, including incineration, reverse osmosis, ozonation, adsorption, solid-phase filtering and coagulation. However, incineration produces toxic volatile byproducts and necessitates extended treatment times; likewise, the stability of ozone is a cause for concern due to its sensitivity to changes in the pH, salt concentration and temperature [26]. The other conventional techniques are also not very efficient in the removal of water contaminants. On the other hand, advanced oxidation processes (AOPs) can efficiently degrade organic contaminants [27–29]. The mechanism of AOPs depends on the production of extremely reactive oxidant substances, particularly $^{\bullet}OH$ [3]. These oxidant species can interact with hazardous substances and cause their destruction [30]. Among various AOPs, $UV/H_2O_2$ and $UV/H_2O_2/Fe^{2+}$ processes have been largely studied for water decontamination due to their simplicity and efficient nature. The $UV/H_2O_2/Fe^{2+}$ process is commonly known as the photo-Fenton process. Both the $UV/H_2O_2$ and $UV/H_2O_2/Fe^{2+}$ processes are capable of producing $^{\bullet}OH$ in the reaction system. In the photo-Fenton process, the $H_2O_2$ and $Fe^{2+}$ react with each other to produce $^{\bullet}OH$ [31]. The $^{\bullet}OH$ reacts with organic pollutants, with the second-order rate constant ranging from $10^6$ to $10^9$ $M^{-1}$ $s^{-1}$ non-selectively [32].

The present research set out to examine the effectiveness of the UV, $UV/H_2O_2$ and $UV/H_2O_2/Fe^{2+}$ processes for the removal of MB. The breakdown efficacy of MB was tested at various pH values and at different initial concentrations of $H_2O_2$, MB and $Fe^{2+}$. In addition, the impact of inorganic anions such as $Cl^-$, $NO_3{}^-$, $CO_3{}^{2-}$ and $HCO_3{}^-$ on the removal of MB was also studied. The degradation products (DPs) of MB were detected and possible degradation pathways were established. Finally, the toxicity of the detected DPs was determined by using a computational program called the Ecological Structure–Activity

Relationships (ECOSAR) program. Density functional theory (DFT) was used to obtain further insights into the reactive centers of MB molecules and to achieve a comprehensive understanding of the degradation pathways of MB by hydroxyl radical-based AOPs.

## 2. Results and Discussion

### *2.1. Direct Photolysis*

To produce hydroxyl radicals and aqueous electrons from water molecules via UV light, photons with a wavelength of 185 nm are required [33]. According to previous reports, for organic molecules to go through direct photolysis, two requirements must be satisfied: (i) the organic molecules must absorb the light photons at the given wavelength to produce electronically excited state molecules (Equation (1)) and (ii) the excited-state molecules must undergo chemical decomposition (Equation (2)) at a higher rate than their physical deactivation (Equation (3)) [34]. According to previous reports, UV 254 nm light can excite the aromatic ring, so MB, being an aromatic compound, could be excited and degraded by UV 254 nm light, as observed in the present study (Figure 1) [35].

$$\text{Methylene blue} + h\nu \rightarrow \text{Methylene blue}^{*} \quad (1)$$

$$\text{Methylene blue}^{*} \rightarrow \text{Degradation products} \quad (2)$$

$$\text{Methylene blue}^{*} \rightarrow \text{Methylene blue} \quad (3)$$

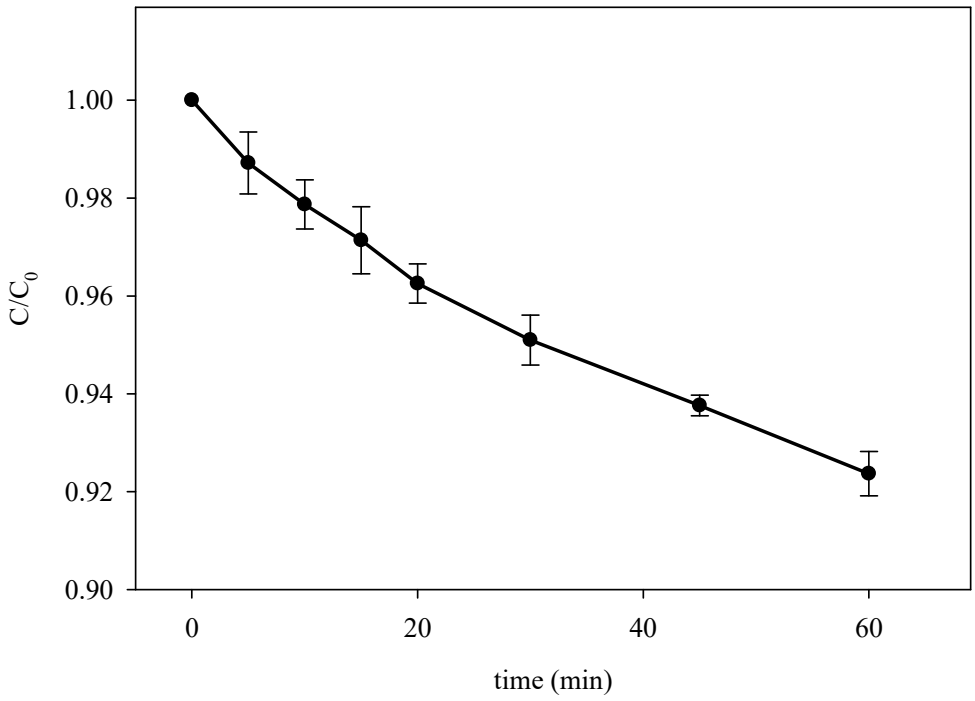


**Figure 1.** Photolytic degradation of methylene blue by UV radiation. Experimental conditions: $[MB]_0$ = 15 mg/L, pH = 6.0.

Applying the *pseudo-first-order* kinetics to MB photolysis, its degradation rate can be written as

$$-\frac{d[MB]}{dt} = k\,[MB] \quad (4)$$

Upon integration, Equation (4) becomes

$$-\ln\frac{[MB]}{[MB]_0} = k_{obs}t \quad (5)$$

where $[MB]_0$ represents the initial concentration of MB, while [MB] represents the MB concentration at time 't'. The molar extinction coefficient ($\varepsilon_{MB}$, $M^{-1}$ $cm^{-1}$) generally affects the direct photolysis of the target compounds and hence their quantum yield ($\phi$) in accordance with Equation (6) [36].

$$\phi_{EMB} = \frac{10U_\lambda \, k_{obs}}{\varepsilon_{MB} \ln(10)} \quad (6)$$

where $k_{obs}$ is in unit of $min^{-1}$, and $U_\lambda$ is the energy of one mole of photons (J $Einstein^{-1}$) at the wavelength of UV radiation, i.e., 471,528 J $Einstein^{-1}$ at 254 nm [36]. By using the Beer–Lambert law (A = ε lc), $\varepsilon_{MB}$ was determined by plotting the concentration versus absorbance. $k_{obs}$ was calculated from the slope of the plot of $-\ln [MB]/[MB]_0$ versus time. The slope was equal to $\varepsilon_{MB}$ because the path length was 1 cm, and the intercept of the plot was set as 0. The $\varepsilon_{MB}$ and $\phi_{MB}$ values were calculated as 15,246 $M^{-1}$ $cm^{-1}$ and 0.7833, respectively.

### *2.2. Removal of MB by UV/$H_2O_2$ and UV/$H_2O_2$/$Fe^{2+}$ Processes*

#### 2.2.1. Impact of $H_2O_2$ Concentration

Both the UV/$H_2O_2$ and UV/$H_2O_2$/$Fe^{2+}$ processes produce $^{\bullet}OH$, as shown in reactions (7)–(12) [37–39]. Therefore, these processes are known as hydroxyl radical-based AOPs.

$$H_2O_2 + h\nu \rightarrow 2\,{}^{\bullet}OH \qquad (\phi = 1.0) \quad (7)$$

$$H_2O_2 + Fe^{2+} \rightarrow {}^{\bullet}OH + OH^- + Fe^{3+} \quad (8)$$

$$Fe^{3+} + H_2O_2 \rightarrow Fe\,(OOH)^{2+} + H^+ \quad (9)$$

$$Fe\,(OOH)^{2+} \rightarrow Fe^{2+} + OOH \quad (10)$$

$$H_2O_2 + Fe^{2+} \rightarrow {}^{\bullet}OH + Fe^{III}\,(OH)^{2+} \quad (11)$$

$$Fe^{III}\,(OH)^{2+} + h\nu \rightarrow {}^{\bullet}OH + Fe^{2+} \quad (12)$$

The photo-Fenton system is able to work continuously via the regeneration of $Fe^{2+}$ in accordance with reactions (10) and (12), and the catalytic reaction proceeds until the consumption of all $H_2O_2$ molecules.

In the present study, a set of experiments was performed with various $H_2O_2$ concentrations (1, 3, 5 and 10 mM) for the removal of MB by the UV/$H_2O_2$ technique at pH 6.0, using 15 mg/L of MB. The findings are depicted in Figure 2. The removal of MB was found to be greatly improved when using the UV/$H_2O_2$ process compared to that by direct photolysis. The % degradation was found to be 70.28, 86.12 and 96.44% in the presence of 1, 3 and 5 mM of $H_2O_2$ at 60 min of irradiation when employing $[MB]_0$ = 15 mg/L and pH = 6.0 (Figure 2a). The reason behind the increase in the degradation of MB is the production of $^{\bullet}OH$ in the UV/$H_2O_2$ process, as shown in reaction (7). The rapid reaction of $^{\bullet}OH$, which is highly reactive and non-selective, with MB led to its degradation. The removal process was accelerated when the amount of $H_2O_2$ in the reaction solution increased, because a larger amount of $^{\bullet}OH$ is formed at a higher concentration of $H_2O_2$, which resulted in the increased % degradation of MB. However, at a 10 mM $H_2O_2$ concentration, the MB degradation was noted to be 91.42%—lower than that at 5 mM $H_2O_2$ (i.e., 96.44%)—suggesting that increases in the $H_2O_2$ concentration beyond 5 mM have a negative impact on the degradation efficiency of MB. Higher concentrations of $H_2O_2$ reduce the effectiveness of MB degradation because $H_2O_2$ scavenges $^{\bullet}OH$ [36]. The values of $k_{obs}$ were calculated to be 0.0285, 0.0371, 0.0556 and 0.0515 $min^{-1}$ at 1, 3, 5 and 10 mM of $H_2O_2$, respectively. The non-linear relationship between the initial $H_2O_2$ concentration and $k_{obs}$ could be due to the scavenging effect of $H_2O_2$- at a higher concentration- for $^{\bullet}OH$, as shown in reaction (13) [40,41]. The hydroperoxyl radical ($HO_2^{\bullet}$)—produced during reaction (13)—has much lower oxidation

capabilities than •OH [42]. $HO_2$• can also consume •OH (reaction (14)), thereby inhibiting the removal efficiency of MB [43].

$$\text{•OH} + H_2O_2 \rightarrow HO_2\text{•} + H_2O \qquad k = 2.7 \times 10^7\ M^{-1}\ s^{-1} \tag{13}$$

$$HO\text{•} + HO_2\text{•} \rightarrow O_2 + H_2O \tag{14}$$

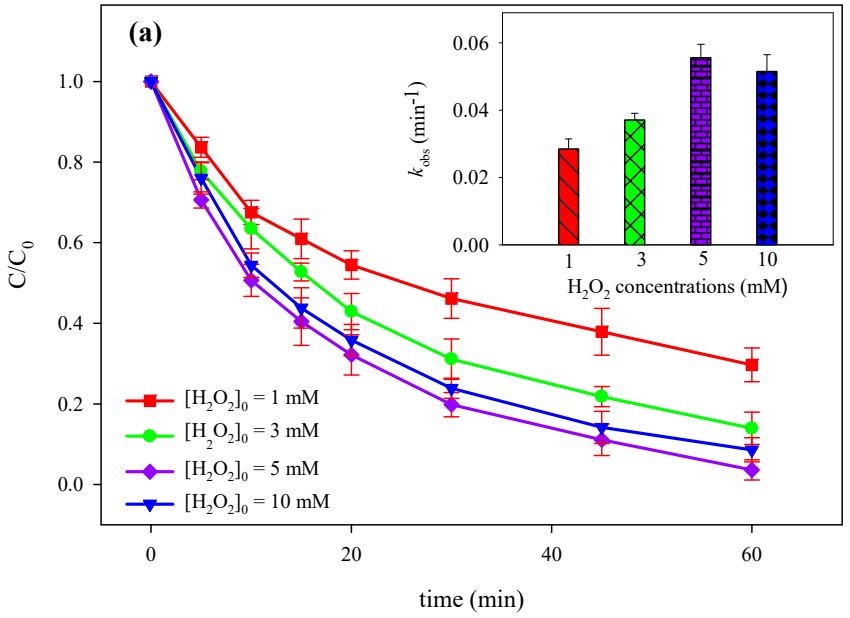


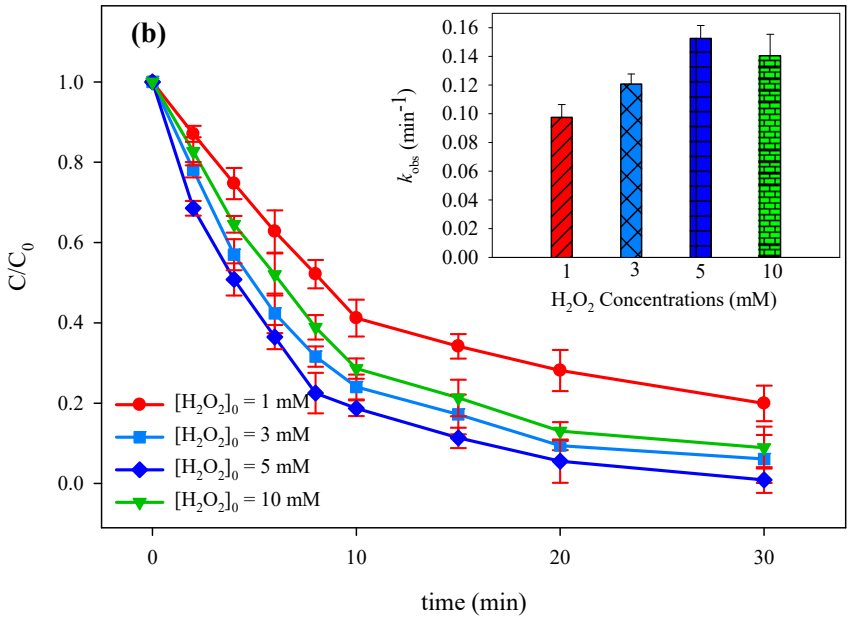


**Figure 2.** Influence of initial concentration of $H_2O_2$ on % removal of methylene blue (MB) by (**a**) UV/$H_2O_2$ and (**b**) UV/$H_2O_2$/$Fe^{2+}$. Reaction conditions: $[MB]_0$ = 15 mg/L, $[Fe^{2+}]_0$ = 0.5 mg/L, pH = 6.0 for UV/$H_2O_2$ and 3.0 for UV/$H_2O_2$/$Fe^{2+}$.

Furthermore, the combination of •OH (reaction (15)) could also negatively impact the degradation of MB at higher $H_2O_2$ concentrations [44].

$$HO\text{•} + HO\text{•} \rightarrow H_2O_2 \qquad k = 5.3 \times 10^9\ M^{-1}\ s^{-1} \tag{15}$$

Reactions (13)–(15) show the consumption of •OH by means other than the reaction of •OH with MB. Therefore, the oxidation of MB was decreased due to these unwanted side reactions at higher $H_2O_2$ concentrations. Hence, determining the appropriate amount of $H_2O_2$ is a crucial step in optimizing the procedure to prevent excess amounts of reagent/oxidant, which could hinder the removal process.

The initial concentrations of $H_2O_2$ in the UV/$H_2O_2$/$Fe^{2+}$ process were the same as those examined in the UV/$H_2O_2$ process, i.e., 1, 3, 5 and 10 mM. The % degradation of MB was found to be 80.68, 91.06, 99.1 and 93.8% when using 1, 3, 5 and 10 mM of $H_2O_2$, respectively (Figure 2b). The initial concentration of MB was 15 mg/L, that of $Fe^{2+}$ was 0.5 mg/L and the pH was 3.0. An acidic pH is used to maintain optimal efficiency in the photo-Fenton system. This is because the catalytic activity of $Fe^{2+}$ in activating $H_2O_2$ has been found to be the maximum at an acidic pH [40]. The values of $k_{obs}$ were observed to be 0.0975, 0.1207, 0.150 and 0.1287 $min^{-1}$ when using 1, 3, 5 and 10 mM of $H_2O_2$, respectively. The findings indicated that as the initial concentration was increased from 1 to 10 mM of $H_2O_2$, a similar trend was observed in this process as observed in the UV/$H_2O_2$ process.

#### 2.2.2. Effect of Initial MB Concentration

To evaluate the influence of the initial MB concentration on its % removal by the UV/$H_2O_2$ and UV/$H_2O_2$/$Fe^{2+}$ processes, methylene blue degradation was studied at an initial concentration of 5, 15 and 20 mg/L, while keeping $[H_2O_2]_0$ = 5 mM and $[Fe^{2+}]_0$ = 0.5 mg/L. In the case of the UV/$H_2O_2$ process, the degradation of MB was found to be 98.64, 96.96 and 82.39% at the irradiation time of 60 min when using 5, 10 and 20 mg/L of MB, respectively, and employing 5 mM of $H_2O_2$ and pH 6.0 (Figure 3a). The removal of MB followed the *pseudo-first-order* kinetics, with the values of $k_{obs}$ being 0.0711, 0.056 and 0.0289 $min^{-1}$ at 5, 15 and 20 mg/L of MB, respectively. For UV/$H_2O_2$/$Fe^{2+}$, the degradation was found to be 100, 99.10 and 89.34% after 30 min of treatment when the concentration of MB was 5, 15 and 20 mg/L, respectively (Figure 3b), employing 5 mM $H_2O_2$, 0.5 mg/L $Fe^{2+}$ and pH 3.0. The $k_{obs}$ values were found to be 0.1923, 0.1473 and 0.1021 $min^{-1}$ for 5, 15 and 20 mg/L of MB, respectively. These findings clearly show that the degradation of MB is reduced when increasing the MB concentration in both the UV/$H_2O_2$ and UV/$H_2O_2$/$Fe^{2+}$ processes. Since both of these processes are based on •OH and the source of •OH (i.e., $H_2O_2$) is also the same in both processes, the reasons for the decreased removal efficiency of MB in both processes could also be the same. There are several reasons for the lower degradation efficiency of MB at a higher concentration. First, at higher MB concentrations, the color of the solution is intense; it then acts as a filter for the UV light, hence preventing the light from entering the solution. Second, the regeneration rate of the $Fe^{2+}$ catalyst from $Fe^{3+}$ via reactions (10)–(12) decreases as the concentration of MB increases due to the reduced penetration of UV light into the reaction solution. The reduced penetration of UV light into the reaction mixture leads to a reduction in the activation of $H_2O_2$ molecules via reactions (7) and (8) and hence smaller quantities of •OH are produced in the reaction solution. This ultimately leads to the lower degradation efficacy of MB at a higher concentration. Another reason for the reduced removal efficacy of MB at a higher concentration is the increased level of intermediate molecules (degradation products of MB) at higher MB concentrations. These intermediate molecules compete with MB for •OH and hence reduce the likelihood of •OH degrading MB, which ultimately results in the lower removal efficiency of MB. The same results were also observed by El-Dein et al. [45] and Navarro et al. [46].

However, the degradation rate of MB increased with an increasing initial concentration of MB. As the initial concentration of MB was increased, a large number of MB molecules were exposed to the reactive radicals, which led to the removal of a larger number of MB molecules at a higher concentration. As a result, a larger number of MB molecules underwent degradation per unit time at a higher MB concentration, which led to a higher degradation rate of MB at a higher concentration [37,47].

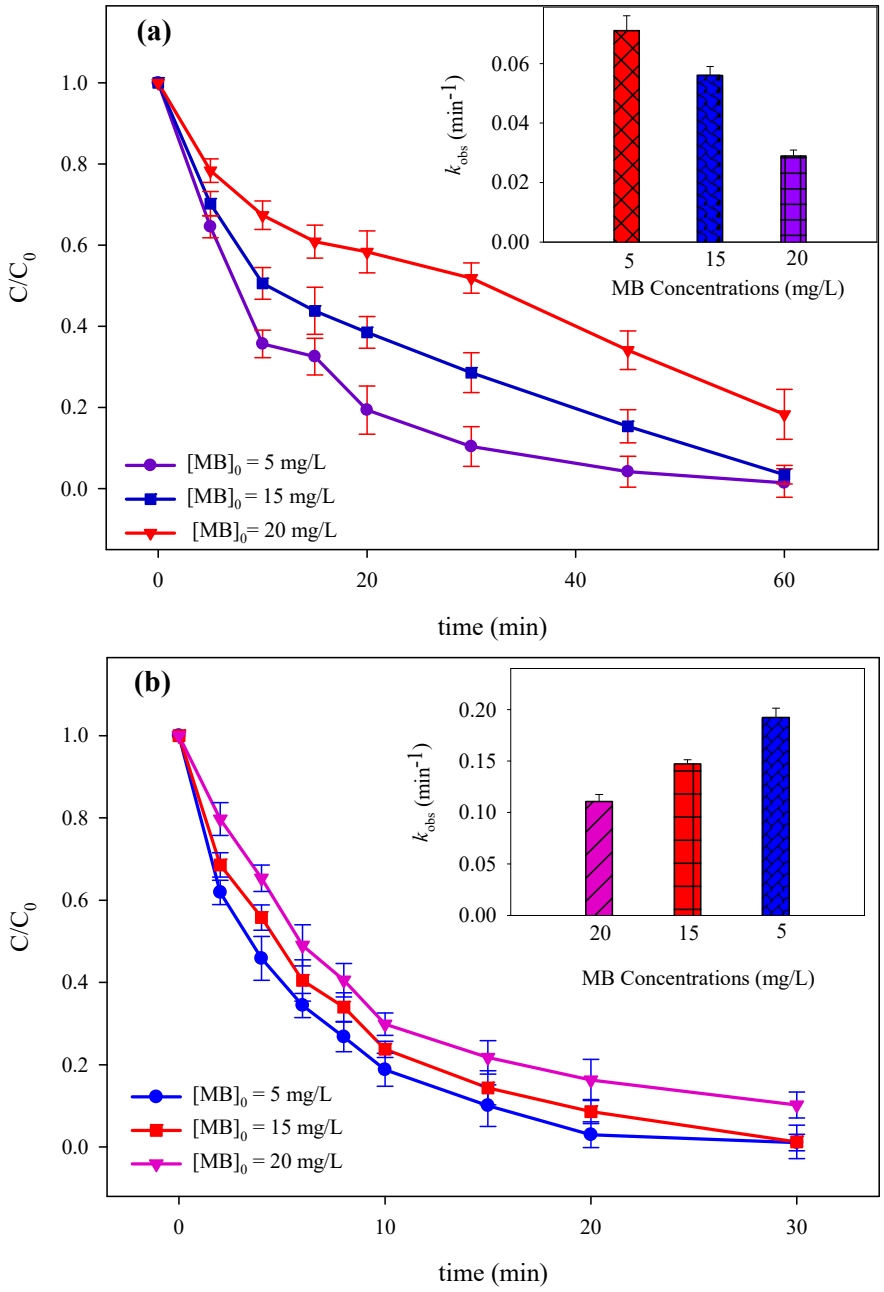


**Figure 3.** Impact of initial concentration of methylene blue on its % degradation by UV/$H_2O_2$ (**a**) and UV/$H_2O_2$/$Fe^{2+}$ processes (**b**). Reaction conditions: $[H_2O_2]_0$ = 5 mM, $[Fe^{2+}]_0$ = 0.5 mg/L, pH = 6.0 (in case of UV/$H_2O_2$) and 3.0 (in case of UV/$H_2O_2$/$Fe^{2+}$).

### 2.2.3. Effect of Inorganic Anions

Various inorganic ions are always present in actual water samples [48]. Therefore, the degradation efficacy of a target contaminant by any AOP could be affected by these ions. As a result, it is essential to understand the efficacy of the water treatment technology in terms of the removal of the target contaminants in the presence of these ions before the recommendation of the investigated technology for practical water treatment applications. In this regard, the present work examined the effects of several inorganic anions, such as chloride ($Cl^-$), nitrate ($NO_3^-$), bicarbonate ($HCO_3^-$) and carbonate ($CO_3^{2-}$) ions, on the removal efficiency of MB by the UV/$H_2O_2$ process and UV/$H_2O_2$/$Fe^{2+}$ system. The findings are depicted in Table 1. The addition of 5 mM $Cl^-$ and $NO_3^-$ reduced the removal of MB from 96.44 (no ions) to 87.13 and 90.19%, respectively. Similarly, for the UV/$H_2O_2$/$Fe^{2+}$ process, the degradation was reduced from 99.11 to 80.56 and 87.46%, respectively, when

5 mM of $Cl^-$ and $NO_3^-$ were added to the MB solution. These findings show that both $Cl^-$ and $NO_3^-$ have minor reduction effects on the removal of MB by UV/$H_2O_2$. Chloride ions are supposed to be effective scavengers for $^\bullet$OH (reaction (16)) [49]. The lower inhibition effect of $Cl^-$ on the removal of MB may be due to the reversibility of reaction (16), which reproduces hydroxyl radicals in a reverse reaction with a slightly higher rate constant ($k_r$) than that of the forward reaction (scavenging of $^\bullet$OH). Moreover, the formation of chlorine radicals ($Cl^\bullet$ and $Cl_2^{\bullet-}$), as a result of reactions (17) and (18), could also reduce the inhibitory effect of $Cl^-$ due to the possible reactivity of MB with $Cl^\bullet$ and $Cl_2^{\bullet-}$.

$$Cl^- + {}^\bullet OH \rightleftharpoons ClOH^{\bullet-} \qquad k_{f\,=}\ 4.3 \times 10^9\ M^{-1}\ s^{-1}, k_r = 6.1 \times 10^9\ M^{-1}\ s^{-1} \quad (16)$$

$$H^+ + ClOH^{\bullet-} \rightleftharpoons Cl^\bullet + H_2O \qquad k_f = 2.6 \times 10^{10}\ M^{-1}\ s^{-1}, k_r = 3.6 \times 10^3\ M^{-1}\ s^{-1} \quad (17)$$

$$Cl^\bullet + Cl^- \rightarrow Cl_2^{\bullet-} \quad (18)$$

**Table 1.** Impact of $Cl^-$, nitrate, carbonate and bicarbonate ions on % removal and $k_{obs}$ of MB by UV/$H_2O_2$ and UV/$H_2O_2$/$Fe^{2+}$ processes. Reaction conditions: $[MB]_0$ = 15 mg/L, $[H_2O_2]_0$ = 5 mM, $[Fe^{2+}]_0$ = 0.5 mg/L, $[NO_3^-] = [Cl^-] = [CO_3^{2-}] = [HCO_3^-]$ = 5 mM. pH was 6.0 for UV/$H_2O_2$ and 3.0 for UV/$H_2O_2$/$Fe^{2+}$. In the presence of $CO_3^{2-}$ and $HCO_3^-$, the pH was 8.2 for UV/$H_2O_2$.

| Anion | UV/$H_2O_2$ | | UV/$H_2O_2$/$Fe^{2+}$ | |
|---|---|---|---|---|
| | % Degradation at 60 Min of Treatment | $k_{obs}$ ($min^{-1}$) | % Degradation at 30 Min of Treatment | $k_{obs}$ ($min^{-1}$) |
| No scavenger | 96.44 | 0.0556 | 99.11 | 0.155 |
| Nitrate ions | 90.19 | 0.0378 | 87.46 | 0.1053 |
| Chloride ions | 87.13 | 0.0361 | 80.56 | 0.093 |
| Carbonate ions | 98.12 | 0.0664 | ----- | ----- |
| Bicarbonate ions | 97.55 | 0.0597 | ----- | ----- |

Furthermore, the presence of $Fe^{2+}$ in UV/$H_2O_2$/$Fe^{2+}$ could also contribute to the reduced removal of MB by $Cl^-$ (reaction (19)) [50,51].

$$Fe^{2+} + ClOH^{\bullet-} \rightarrow Fe^{3+} + Cl^- + OH^- \quad (19)$$

The effect of nitrate ions ($NO_3^-$) on MB degradation via the UV/$H_2O_2$ and UV/$H_2O_2$/$Fe^{2+}$ processes could also be explained by the fact that $NO_3^-$ could also act as an $^\bullet$OH radical scavenger (reaction (20)) [48,52].

$$NO_3^- + {}^\bullet OH \rightarrow {}^-OH + NO_3^\bullet \quad (20)$$

However, $CO_3^{2-}$ and $HCO_3^-$ were found to have positive impact on the degradation of MB (Table 1). The % degradation was increased from 96.44 to 98.12 and 97.55% when 5 mM of $CO_3^{2-}$ or 5 mM of $HCO_3^-$ was added to the solution, respectively, for the UV/$H_2O_2$ system (Table 1). Some previous studies have also reported the higher degradation of Acid Orange II (AO7) and basic fuchsin dyes by the UV/$H_2O_2$ process in the presence of $CO_3^{2-}$ and $HCO_3^-$ [53,54]. This could be due to the activation of $H_2O_2$ by $CO_3^{2-}$ and $HCO_3^-$. Although $CO_3^{2-}$ and $HCO_3^-$ can scavenge $^\bullet$OH, they could in turn lead to the formation of carbonate radicals ($CO_3^{\bullet-}$) (reactions (21) and (22)). $CO^\bullet{}_3^-$ is also considered a reactive species, with redox potential of 1.59 V, and hence can degrade organic dyes [55]. It has been reported that $CO_3^{\bullet-}$ reacts strongly with sulfur-containing compounds and electron-rich compounds such as MB, with a second-order rate constant in the order of $10^6$–$10^8$ $M^{-1}$ $s^{-1}$ [56]. As a result, $CO_3^{2-}$ and $HCO_3^-$ did not show any negative effect on MB degradation by UV/$H_2O_2$ but rather a positive effect, i.e., the higher removal of MB was found in the presence of these ions. Another possible reason for the higher removal of MB in the presence of $HCO_3^-$ is the formation of peroxymonocarbonate ions ($HCO_4^-$) resulting from the reaction of $H_2O_2$ with $HCO_3^-$ (reaction (23)) [56]. $HCO_4^-$,

produced in situ, is highly unstable at room temperature and is split into reactive species such as superoxide radical anions ($O_2^{\bullet-}$). Due to its significant oxidizing ability in the breakdown of contaminants, this $O_2^{\bullet-}$ has the potential to degrade the target dye— in this case, MB [57]. Additionally, the recombination rate of $CO_3^{\bullet-}$ is 275 times lower than that of $^{\bullet}OH$, making it more available for the degradation of MB [56]. In conclusion, despite the consumption of $^{\bullet}OH$ by $CO_3^{2-}$ and $HCO_3^-$, the % degradation of MB was increased.

$$CO_3^{2-} + {}^{\bullet}OH \rightarrow {}^{-}OH + CO_3^{\bullet-} \qquad k = 3.9 \times 10^8\ M^{-1}\ s^{-1} \tag{21}$$

$$HCO_3^- + {}^{\bullet}OH \rightarrow CO_3^{\bullet-} + H_2O \qquad k = 8.5 \times 10^6\ M^{-1}\ s^{-1} \tag{22}$$

$$H_2O_2 + HCO_3^- \rightarrow HCO_4^- + H_2O \tag{23}$$

For the UV/$H_2O_2$/$Fe^{2+}$ process, however, the effects of $CO_3^{2-}$ and $HCO_3^-$ were not evaluated because both of these ions render the reaction solution alkaline, and the activity of $Fe^{2+}$ is negligible as a catalyst for $H_2O_2$ activation due to the formation of ferrous hydroxide at a higher pH in the solution [58].

#### 2.2.4. Effect of pH

One of the most critical factors affecting the degradation efficiency of water treatment methods is the pH. Hence, the efficiency of the UV/$H_2O_2$ process was assessed at pH 3.0, 6.0 and 11 and that of UV/$H_2O_2$/$Fe^{2+}$ at pH 3.0 and 6.0. The findings showed that the pH affected the degradation of MB by both processes (Figure 4a). The degradation efficiency of UV/$H_2O_2$ was found to be higher at pH 6.0, as evidenced by the 89.82, 96.44 and 77.62% degradation of MB at pH 3.0, 6.0 and 11, respectively, at irradiation time = 60 min, $[H_2O_2]_0$ = 5 mM and $[MB]_0$ = 15 mg/L. Accordingly, $k_{obs}$ was calculated to be 0.0468, 0.0556 and 0.0378 $min^{-1}$ at pH 3.0, 6.0 and 11, respectively. The relatively lower efficiency at pH 3 as compared to pH 6 could be due to the scavenging of $^{\bullet}OH$ by $Cl^-$ (from HCl) at pH 3 (reactions (16)–(18)) [59]. $Cl_2^{\bullet-}$ has lower reactivity in comparison to $^{\bullet}OH$ towards organic compounds [60].

Furthermore, the reduced removal of MB at pH 11 is because of the dissociation of $H_2O_2$ to its conjugate base ($HO_2^-$) at a pH higher than 10 (pKa of $H_2O_2$ = 11.62) (reaction (24)).

$$H_2O_2 \rightarrow HO_2^- + H^+ \tag{24}$$

$HO_2^-$, the conjugate anion of $H_2O_2$, reacts with an undissociated $H_2O_2$ molecule to produce oxygen molecules and water, rather than $^{\bullet}OH$, when exposed to UV light. As a result, the concentration of $^{\bullet}OH$ is lower than expected (reaction (25)) [46].

$$HO_2^- + H_2O_2 \rightarrow H_2O + O_2 \tag{25}$$

Moreover, the redox potential of $^{\bullet}OH$ is reported to be 2.7 V at an acidic pH and 1.8 V at a neutral pH [61]. Hence, the lower efficiency at an alkaline pH may be attributed to the decrease in the redox potential of $^{\bullet}OH$.

Furthermore, the UV/$H_2O_2$/$Fe^{2+}$ process showed a strong dependence on the pH. In contrast to the UV/$H_2O_2$ process, the removal efficacy of UV/$H_2O_2$/$Fe^{2+}$ was found to be higher at pH 3.0. The % degradation was found to be 99.11 and 82.91% at pH 3.0 and 6.0, corresponding to the $k_{obs}$ values of 0.1550 and 0.0757 $min^{-1}$, respectively (Figure 4b), when employing 5 mM $H_2O_2$, 15 mg/L MB, 0.5 mg/L $Fe^{2+}$ and 30 min of treatment time. The higher removal efficiency of UV/$H_2O_2$/$Fe^{2+}$ at pH 3.0 is due to the fact that the rate of activation of $H_2O_2$ by $Fe^{2+}$ is high at an acidic pH (reaction (26)). It has been reported that the optimum pH for the degradation efficacy of organic pollutants by UV/$H_2O_2$/$Fe^{2+}$ is 3.0. At a pH less than 2.5 and higher than 4.0, the catalytic role of $Fe^{2+}$ decreases [62]. This is because, at a higher pH, $Fe(OH)_3$ is produced, which reduces the availability of $Fe^{2+}$ to activate $H_2O_2$ for $^{\bullet}OH$ production. Furthermore, the presence of electron donor

reagents such as $Fe^{2+}$ at a very low pH encourages $H^+$ to scavenge $^{\bullet}OH$, thereby inhibiting the degradation of the target compound (reaction (27)) [37,63].

$$H_2O_2 + Fe^{2+} \rightarrow {}^{\bullet}OH + Fe^{3+} + OH^- \quad (26)$$

$$^{\bullet}OH + Fe^{2+} + H^+ \rightarrow H_2O + Fe^{3+} \quad (27)$$

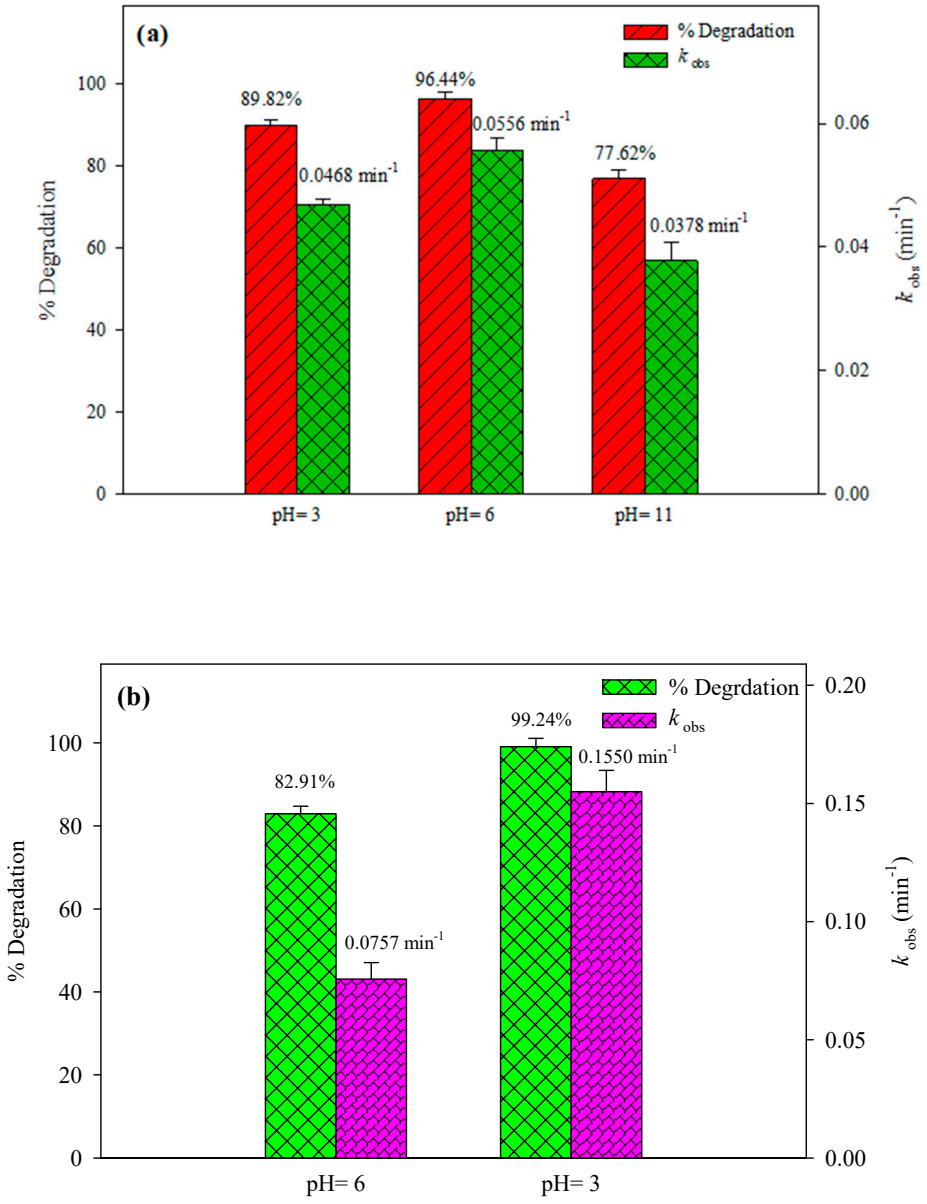


**Figure 4.** (**a**) Influence of pH on % removal of methylene blue by UV/$H_2O_2$ process. Reaction conditions: $[MB]_0$ = 15 mg/L, $[H_2O_2]_0$ = 5 mM, time = 60 min. (**b**) Impact of pH on removal efficiency of methylene blue by UV/$H_2O_2$/$Fe^{2+}$ process. Experimental conditions: $[MB]_0$ = 15 mg/L, $[H_2O_2]_0$ = 5 mM, $[Fe^{2+}]_0$ = 0.5 mg/L, time = 30 min.

### 2.2.5. Influence of Initial Concentration of $Fe^{2+}$

In this study, three initial concentrations of $Fe^{2+}$, i.e., 0.1, 0.2 and 0.5 mg/L, were used to study the impact of the catalytic role of ferrous ions. The removal efficiency of the UV/$H_2O_2$/$Fe^{2+}$ process was found to be enhanced at higher concentrations of $Fe^{2+}$ (Figure 5). The % degradation was found to be 76.78, 93.77 and 99.11% after an irradiation time of 30 min at 0.1, 0.2 and 0.5 mg/L of $Fe^{2+}$, respectively, when employing 15 mg/L of MB, 5 mM of $H_2O_2$ and pH 3.0. In the same way, the values of $k_{obs}$ were observed to be

0.0719, 0.132 and 0.155 $min^{-1}$ at 0.1, 0.2 and 0.5 mg/L of $Fe^{2+}$, respectively. The increase in the % degradation with an increase in the amount of $Fe^{2+}$ could be due to the higher concentration of •OH at higher concentrations of $Fe^{2+}$ via reaction (8) [50,62]. Additionally, there was a linear relation between $k_{obs}$ and the concentration of $Fe^{2+}$.

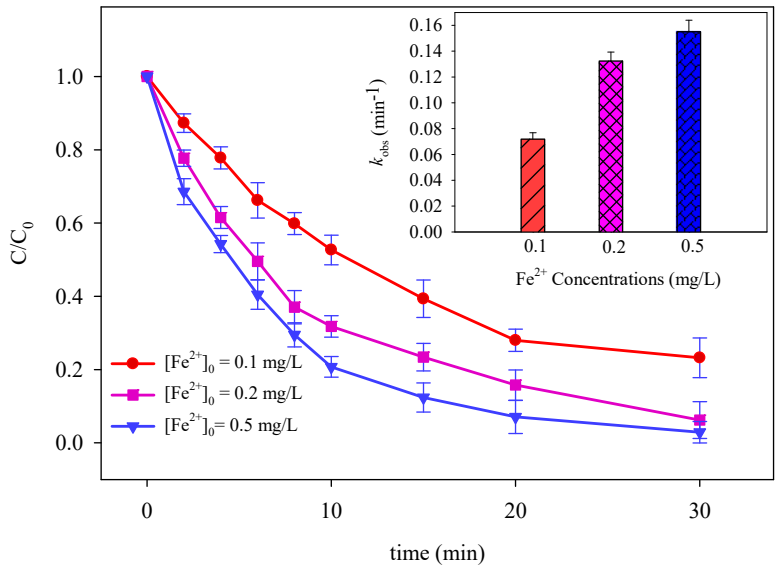


**Figure 5.** Impact of $Fe^{2+}$ concentration on % removal of methylene blue by UV/$H_2O_2$/$Fe^{2+}$ process. Reaction conditions: $[MB]_0$ = 15 mg/L, $[H_2O_2]_0$ = 5 mM, pH = 3.0.

To better illustrate the efficiencies of the AOPs studied in this work in comparison with similar AOPs reported previously for the degradation of MB, we present Table 2. Table 2 serves to enrich the existing knowledge on the removal of MB by the UV/$H_2O_2$ and UV/$H_2O_2$/$Fe^{2+}$ processes.

**Table 2.** Comparison of methylene blue removal by UV/$H_2O_2$ and UV/$H_2O_2$/$Fe^{2+}$ processes.

| Method | Concentration of Methylene Blue (mg/L) | $[H_2O_2]_0$ | $[Fe^{2+}]_0$ | pH | Time (min) | $k_{obs}$ ($min^{-1}$) | Degradation (%) | Reference |
|---|---|---|---|---|---|---|---|---|
| UV/$H_2O_2$ | 15 | 5 mM | ----- | 6 | 60 | 0.0556 | 96.44 | This work |
| UV/$H_2O_2$/$Fe^{2+}$ | 15 | 5 mM | 0.5 mg/L | 3 | 30 | 0.150 | 99.1 | This work |
| UV/$H_2O_2$ | 50 | 12.5 mM | ----- | 3 | 90 | ----- | 91 | [64] |
| UV/$H_2O_2$ | 10 | 15 mL (30% $H_2O_2$) | ----- | ---- | 80 | 0.0082 | ----- | [65] |
| UV/$H_2O_2$ | 10 | 4 mL/L | ----- | ----- | 90 | 0.0770 | ----- | [66] |
| UV/$H_2O_2$ | 10 | 15 mL (10% $H_2O_2$) | ----- | ----- | 60 | ----- | 99.90 | [67] |
| UV/$H_2O_2$/$Fe^{2+}$ | 20 | 70 mM | 4 mM | 3 | ----- | ----- | 97.8 | [68] |
| UV/$H_2O_2$/$Fe^{2+}$ | 50 | 8 mM | 5 mM | | 60 | ----- | 100 | [69] |
| UV/$H_2O_2$/$Fe^{2+}$ | 20 | 70 mM | 4 mM | 3 | 30 | ----- | 98.8 | [70] |

2.2.6. Determination of Degradation Products and Possible Degradation Pathways

The degradation products (DPs) of MB produced during UV/$H_2O_2$ treatment were identified by GC-MS. It is extremely helpful to identify the possible reactive sites of MB where •OH could attack via addition or hydrogen abstraction reactions before discussing the experimentally detected DPs of MB. Therefore, the possible reactive sites of MB towards •OH addition or hydrogen abstraction reactions were identified by performing density functional theory (DFT) calculations using the Gaussian 09 program. In this regard, the B3LYP/3-21g basis set was used for the optimization of MB, whereas the B3LYP/6-311g

basis set was used for energy calculations. In order to forecast the positions in the MB molecule where •OH could readily go through addition or hydrogen abstraction reactions, the frontier electron densities (FEDs) and point charges of the MB atoms were calculated using the Gaussian 09 program. The calculated values of the FEDs and point charges of MB are given in Table 3. According to published reports, •OH could attack via addition reactions on atoms with high values of ($FED^2_{HOMO}$ + $FED^2_{LUMO}$) [47], while hydrogen could be abstracted by •OH from atoms whose point charge values are high [47,71]. Keeping these information in mind, N18 could be the first site to be attacked by •OH via an addition reaction due its large ($FED^2_{HOMO}$ + $FED^2_{LUMO}$) value (i.e., 0.18067) (Table 3). However, according to basic rules of chemistry, the second shell of a nitrogen atom can accommodate a maximum of eight electrons. When •OH attacks at N18, the number of electrons in the valance shell of nitrogen increases from eight to nine, which nitrogen cannot accommodate. The case of N11 is similar, with the next ($FED^2_{HOMO}$ + $FED^2_{LUMO}$) value of 0.18066 (Table 3). Therefore, •OH could preferentially attack N4 via an addition reaction. The next sites of •OH attack via addition reactions are C3 and C4 based on their ($FED^2_{HOMO}$ + $FED^2_{LUMO}$) values, i.e., 0.07854 and 0.07853. Meanwhile, S1 has the highest point charge due to the existence of a positive charge on the sulfur atom (S) resulting from the ionization of the MB molecule. However, S1 has no hydrogen atom to be abstracted by •OH. Similarly, C15 and C8 have the next highest point charge values, but they also do not have hydrogen atoms for abstraction. In addition, C3 and C5 have point charge values of 0.10003 and 0.10002, respectively, and C2 and C6 have the next highest values of −0.1019, but, again, these atoms cannot be attacked by •OH for hydrogen abstraction because these atoms also lack hydrogen to be abstracted. Therefore, the possible hydrogen abstraction sites are proposed to be C17 and C10, as well as C16 and C9, which have the lowest negative values (i.e., relatively large values) of point charges among the atoms bearing hydrogen atoms.

**Table 3.** Frontier electron densities and point charges of MB atoms calculated by Gaussian 09 program.

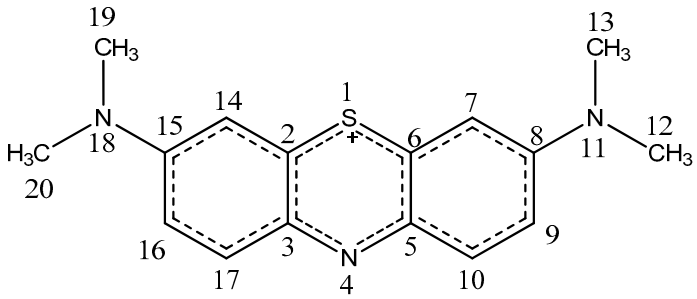


| Atom | $FED^2_{HOMO}$ + $FED^2_{LUMO}$ | Charge | Atom | $FED^2_{HOMO}$ + $FED^2_{LUMO}$ | Charge |
|---|---|---|---|---|---|
| S1 | 0.0847 | 0.39728 | N11 | 0.18066 | −0.3592 |
| C2 | 0.06067 | −0.1019 | C12 | 0.00193 | −0.3701 |
| C3 | 0.07854 | 0.10003 | C13 | 0.00186 | −0.3716 |
| N4 | 0.16829 | −0.3478 | C14 | 0.04223 | −0.2880 |
| C5 | 0.07853 | 0.10002 | C15 | 0.05691 | 0.25335 |
| C6 | 0.06067 | −0.1019 | C16 | 0.04907 | −0.2408 |
| C7 | 0.04223 | −0.2880 | C17 | 0.03981 | −0.1077 |
| C8 | 0.05691 | 0.25335 | N18 | 0.18067 | −0.3592 |
| C9 | 0.04906 | −0.2408 | C19 | 0.00186 | −0.3716 |
| C10 | 0.03981 | −0.1077 | C20 | 0.00193 | −0.3701 |

In the present work, three DPs of MB were identified experimentally by GC-MS, namely 2-amino-5-dimethylamino-benzene sulfonic acid (ADABSA), 4-(dimethylamino)aniline (DMA) and hydroquinone (HQ) (Scheme 1). The •OH could attack at N4 due its high $FED^2_{HOMO}$ + $FED^2_{LUMO}$, producing a sulfoxide group (not detected), but this is supposed to be a tentative product [72]. Due to the low bond energy of 70.8 kcal/mol, during the attack of •OH, demethylation occurs, followed by its oxidation to produce HCHO or HCOOH [73,74].

The further oxidation of MB resulted in the breakdown of the nitrogen–sulfur heterocycle, resulting the generation of ADABSA ($m/z$ = 215) [75]. The oxidation of ADABSA results the generation of DMA ($m/z$ = 136). The subsequent demethylation and deamination reactions and further oxidation by •OH finally lead to the production of HQ ($m/z$ = 110) [73,76]. The mentioned three DPs have also been detected by other researchers while studying the degradation of MB [75,76]. Yu and Barker [49] detected ADABSA through heterogeneous catalysis under visible light irradiation. Ag-$Cu_2O$ was used as a photocatalyst. Similarly, DMA was detected in [72] by the bio-electro-Fenton coupled with microbial desalination cell process. A compound with an $m/z$ value of 110 was detected in [75,76].

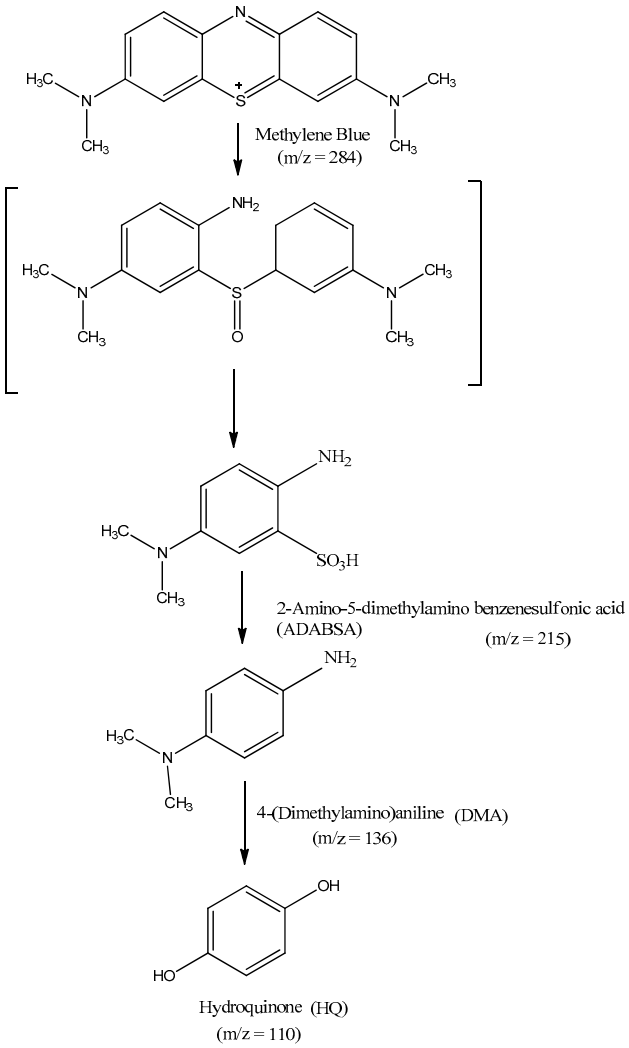


**Scheme 1.** Proposed degradation mechanism of methylene blue by UV/$H_2O_2$ process. The product in square brackets was not detected here but is supposed to be a tentative degradation product.

### 2.2.7. Toxicity Evaluation

The basic aim of water treatment techniques is to achieve clean and pure water, i.e., toxicant-free water. To check whether the toxicity of the treatment mixture was reduced during the degradation of MB, the aquatic toxicity of the identified DPs towards fish, daphnia and green algae was determined using the ECOSAR program (Version 2.2) (Table 4) [77,78]. Surprisingly, DMA, one of the detected DPs, was found to have higher acute toxicity towards daphnia and higher chronic toxicity towards both daphnia and fish than MB. Therefore, it can be concluded that researchers should not only focus on the removal of target compounds while dealing with the removal of dyes. Rather, the toxicity of the treated solution should be determined before, during and after the treatment so as to ensure a

reduction in its toxicity. Moreover, the treatment time should be prolonged such that the treatment technology not only degrades/removes the target pollutant but also the DPs, i.e., until complete mineralization is achieved.

**Table 4.** Aquatic toxicity of malachite green and its identified DPs (unit = mg $L^{-1}$).

| Compound | Acute Toxicity | | | Chronic Toxicity | | |
|---|---|---|---|---|---|---|
| | Fish ($LC_{50}$) | Daphnia ($LC_{50}$) | Green Algae ($EC_{50}$) | Fish (ChV) | Daphnia (ChV) | Green Algae (ChV) |
| MB | 5.79 | 3.88 | 5.72 | 2.38 | 0.599 | 2.16 |
| ADABSA | 82,500 | 225 | 1150 | 4130 | 1.90 | 1590 |
| DMA | 45.1 | 2.20 | 6.52 | 0.616 | 0.025 | 2.42 |
| HQ | 669 | 347 | 179 | 58.2 | 26.4 | 38.4 |

### 2.2.8. Total Organic Carbon Analysis

The detected degradation byproducts (i.e., ADABSA, DMA and HQ) of MB are organic in nature and can be harmful to both humans and aquatic organisms. Therefore, the removal efficiencies of both processes (i.e., $UV/H_2O_2$ and $UV/H_2O_2/Fe^{2+}$) were investigated for the removal of total organic carbon (TOC). It is noted that TOC removal requires more time than that required for the degradation of MB. Furthermore, the TOC analysis was carried out at pH 7.0 and pH 3.0 for the $UV/H_2O_2$ and $UV/H_2O_2/Fe^{2+}$ processes, respectively. After 360 min, $UV/H_2O_2$ was able to remove 59% of the TOC, while $UV/H_2O_2/Fe^{2+}$ removed 71% of the TOC (Figure 6). The higher TOC removal efficiency of $UV/H_2O_2/Fe^{2+}$ could possibly attributed to the higher redox potential (2.7 V) of $^{\bullet}OH$ at an acidic pH than at a neutral pH (1.8 V) [79]. Furthermore, in $UV/H_2O_2/Fe^{2+}$, $H_2O_2$ could be activated by both $Fe^{2+}$ and UV light, while it could be activated by UV light only in the $UV/H_2O_2$ process. Hence, more $^{\bullet}OH$ was expected to be produced by $UV/H_2O_2/Fe^{2+}$ than that produced by the $UV/H_2O_2$ process, which led to higher TOC removal. In addition, $Fe^{2+}$ catalyzed the $^{\bullet}OH$ formation from $H_2O_2$ (reaction (26)), which could be associated with the higher TOC removal efficiency of $UV/H_2O_2/Fe^{2+}$.

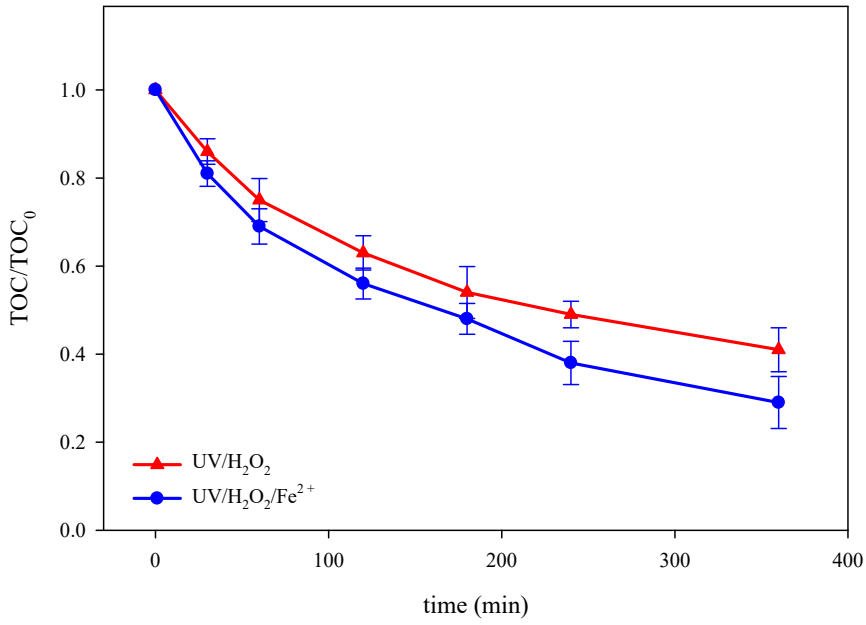


**Figure 6.** Removal of TOC by $UV/H_2O_2$ and $UV/H_2O_2/Fe^{2+}$ processes. Reaction conditions: $[MB]_0$ = 15 mg/L $[H_2O_2]_0$ = 5 mM, $[Fe^{2+}]_0$ = 0.5 mg/L, pH = 6.0 (in case of $UV/H_2O_2$) and 3.0 (in case of $UV/H_2O_2/Fe^{2+}$).

## 3. Chemicals and Methods

### *3.1. Chemicals*

Methylene blue dye and hydrogen peroxide ($H_2O_2$) (30% purity) were obtained from Sigma-Aldrich, Darmstadt, Germany. Sodium hydrogen carbonate ($NaHCO_3$), sodium carbonate ($Na_2CO_3$), potassium chloride (KCl), ferrous sulfate heptahydrate ($FeSO_4 \bullet 7H_2O$) and sodium nitrate ($NaNO_3$) were purchased from BDH. Hydrochloric acid (HCl) (37% purity) and sodium hydroxide (NaOH) were purchased from Merck, Darmstadt, Germany.

### *3.2. Photodegradation*

The photochemical reactor was a 100 mL beaker containing 50 mL of the reaction solution, irradiated by UV radiation. The UV radiation source was a 35 W mercury (Hg, Philips, Warszawa, Poland) lamp that emitted light at λ = 254 nm. The selected concentration of MB was 15 mg/L, if not stated otherwise. The initial pH was adjusted with (HCl) and NaOH in the case of pH 3.0 and 11.0, respectively. The irradiated samples were taken at various time intervals (pre-determined) for quantification analysis. The experiments were repeated three times, and the errors bars represented the standard deviations of the results.

### *3.3. Analytical Methods*

The concentration of MB was monitored using a UV–vis spectrophotometer (Perkin Elmer, Waltham, MA, USA) by measuring its absorbance at 664 nm. The degradation products (DPs) of MB were analyzed by gas chromatography (GC, model 8890, Agilent, Santa Clara, CA, USA) using a mass-spectrometric detector (MS, model 5977, Agilent) equipped with a HP-5 capillary column (30 m × 0.25 mm, 0.25 µm film thickness). The oven temperature was programmed as follows: 80 °C (hold for 2 min), which was then elevated to 200 °C at a rate of 10 °C/min (hold for 2 min) and finally ramped to 280 °C at a rate of 10 °C/min (hold for 3 min). The temperatures of the injector and MS detector were set at 250 °C and 300 °C, respectively. MS analysis was performed in electron impact ionization mode at 70 eV, with the MS scan range from 50 to 450 $m/z$. The carrier gas was He, set at a flow rate of 1.0 mL/min. The DPs were extracted from the treated water samples by dichloromethane. A Shimadzu VCSH-ASI TOC analyzer (S868781) was used for the measurement of TOC removal. For the TOC analysis, 25 mL of the sample volume was used.

Equation (28) was used to determine the degradation efficacy of MB [80].

$$\% \text{ Degradation} = \left[\frac{(C_0 - C_t)}{C_0}\right] \times 100 \quad (28)$$

### *3.4. Frontier Electron Density and Point Charge Calculations*

To find the reactive sites/centers in the MB molecule where $^{\bullet}$OH could preferentially attack, the frontier electron densities (FEDs) of the molecular orbitals of MB and the point charges of the C- and N-atoms were calculated using the Gaussian 09 program. FED calculations were performed for both the highest occupied molecular orbitals (HOMOs) and the lowest unoccupied molecular orbitals (LUMOs). Initially, the geometry of MB was optimized using density functional theory with the B3LYP/3-21g basis set. Thereafter, the energy calculations for FED and point charge determination were performed with the hybrid B3LYP method of density functional theory (DFT) with the 6-311g basis set (B3LYP/6-311g).

### *3.5. Toxicity Investigation*

The tool known as Ecological Structure–Activity Relationships (ECOSAR) was utilized in order to determine the acute and chronic toxicities of MB, as well as its degradation products (DPs). ECOSAR is supposed to be an excellent method for the prediction of the aquatic toxicity of hazardous contaminants [49]. The ECOSAR program can be used to

evaluate both the chronic and acute toxicities of compounds with toxicity towards fish and daphnia, as well as green algae. This program evaluates the acute toxicity in terms of the $LC_{50}$ and $EC_{50}$. The $LC_{50}$ is the toxicant concentration that can cause the death of 50% fish and 50% daphnia after 96 and 48 h exposure, respectively. The $EC_{50}$ is the concentration of the toxicant responsible for the 50% growth inhibition of green algae after an exposure time of 96 h [79].

## 4. Conclusions

The aim of this study was the degradation of MB, a toxic dye discharged by the textile industry, through the UV/$H_2O_2$ and UV/$H_2O_2$/$Fe^{2+}$ techniques. Only 6.318% MB degradation was observed after 60 min under UV alone. The impact of the initial concentrations of $H_2O_2$ and $Fe^{2+}$ was evaluated regarding the degradation of MB by adding various concentrations of $H_2O_2$ (1, 3, 5 and 10 mM) and 0.1, 0.2 and 0.5 mg/L of $Fe^{2+}$ to the 15 mg/L MB solution. The degradation efficiency was synergistically increased in both the UV/$H_2O_2$ and UV/$H_2O_2$/$Fe^{2+}$ processes. After 60 min of treatment, 96.44% degradation was achieved using the UV/$H_2O_2$ process, whereas 99.11% degradation was achieved for the UV/$H_2O_2$/$Fe^{2+}$ process. $Fe^{2+}$ was found to accelerate the degradation of MB, especially at pH 3.0, resulting in a photo-Fenton system. Inorganic anions such as $NO_3^-$ and $Cl^-$ reduced the degradation of MB by UV/$H_2O_2$ from 96 to 90.19 and 87.13%, while, in the case of UV/$H_2O_2$/$Fe^{2+}$, the degradation was reduced from 99.11 to 87.46 and 80.56% in the presence of 5 mM of each ion. However, $CO_3^{2-}$ and $HCO_3^-$ enhanced the removal of MB by UV/$H_2O_2$ due to the formation of $CO_3^{\bullet-}$ and other secondary radicals, which play important role in the degradation of MB. The computational aquatic toxicity study on three aquatic organisms (fish, daphnia and green algae) showed that DMA (one of the detected DPs) was more toxic than MB. Furthermore, the UV/$H_2O_2$ and UV/$H_2O_2$/$Fe^{2+}$ processes showed significant TOC removal efficiencies of 59% and 71%, respectively. The present study reveals that MB can effectively be degraded by hydroxyl radical-based AOPs; however, researchers should also ensure the complete removal of its DPs so that the toxicity of the treated water does not increase due to the formation of toxic DPs.

**Author Contributions:** Conceptualization, W.A., R.S. and D.K.; Data curation, W.A. and D.K.; Formal analysis, W.A., R.S. and H.U.H.; Investigation, W.A., R.S. and H.U.H.; Methodology, W.A. and D.K.; Writing—original draft, W.A., R.S., H.U.H. and D.K.; Resources, D.K., S.K., A.A.-A. and C.H.; Software, S.K.; Validation, S.K., A.A.-A. and J.A.K.; Writing—review and editing, S.K., A.A.-A., J.A.K., N.R.B.R. and C.H.; Funding acquisition, A.A.-A., J.A.K. and C.H.; Project administration, J.A.K.; Supervision, J.A.K. All authors have read and agreed to the published version of the manuscript.

**Funding:** The Higher Education Commission (HEC), Pakistan, funded this work through the National Research Program for Universities (NRPU) Project, Ref No. 20-15851/NRPU/R&D/HEC/2021-2020. The Researchers Supporting Project Number RSPD2024R534, King Saud University, Riyadh, Saudi Arabia also provided funds for this work. In addition, this study was funded by a National Research Foundation of Korea (NRF) grant funded by the Korean government (MSIT) (No. 2021R1A2C1093183) and the Korean–American Educational Commission, funded by the U.S. and Korean Governments.

**Data Availability Statement:** The data presented in this study are available in this article.

**Acknowledgments:** The authors gratefully acknowledge the financial support of Abdul Wali Khan University Mardan, Pakistan, through the Research Innovation Fund (RIF). The Higher Education Commission (HEC), Pakistan, is highly acknowledged for the financial support through the National Research Program for Universities (NRPU) Project, Ref No. 20-15851/NRPU/R&D/HEC/2021-2020. The authors also gratefully acknowledge the Researchers Supporting Project Number RSPD2024R534, King Saud University, Riyadh, Saudi Arabia. C.H. acknowledges the support of the National Research Foundation of Korea (NRF) grant funded by the Korean government (MSIT) (No. 2021R1A2C1093183) and the research support provided through a Fulbright Visiting Scholar Award from the Korean–American Educational Commission, funded by the U.S. and Korean Governments.

**Conflicts of Interest:** The authors declare that they have no known competing financial interests or personal relationships that could have appeared to influence the work reported in this paper.

## References


1. Ali, I.; Mbianda, X.; Burakov, A.; Galunin, E.; Burakova, I.; Mkrtchyan, E.; Tkachev, A.; Grachev, V. Graphene based adsorbents for remediation of noxious pollutants from wastewater. *Environ. Int.* **2019**, *127*, 160–180. [CrossRef] [PubMed]
2. Alqadami, A.A.; Naushad, M.; Abdalla, M.A.; Ahamad, T.; Alothman, Z.A.; Alshehri, S.M.; Ghfar, A.A. Efficient removal of toxic metal ions from wastewater using a recyclable nanocomposite: A study of adsorption parameters and interaction mechanism. *J. Clean. Prod.* **2017**, *156*, 426–436. [CrossRef]
3. Papić, S.; Koprivanac, N.; Božić, A.L.; Vujević, D.; Dragičević, S.K.; Kušić, H.; Peternel, I. Advanced oxidation processes in azo dye wastewater treatment. *Water Environ. Res.* **2006**, *78*, 572–579. [CrossRef] [PubMed]
4. Liu, R.; Ji, W.; Min, J.; Wen, P.; Li, Y.; Hu, J.; Yin, L.; He, G. Efficient Removal of Cationic Dye by Biomimetic Amorphous Calcium Carbonate: Behavior and Mechanisms. *Molecules* **2024**, *29*, 5426. [CrossRef]
5. Yin, X.; Jiang, Y.; Tan, Y.; Meng, X.; Sun, H.; Wang, N. Co-transport of graphene oxide and heavy metal ions in surface-modified porous media. *Chemosphere* **2019**, *218*, 1–13. [CrossRef]
6. Jamee, R.; Siddique, R. Biodegradation of synthetic dyes of textile effluent by microorganisms: An environmentally and economically sustainable approach. *Eur. J. Microbiol. Immunol.* **2019**, *9*, 114–118. [CrossRef] [PubMed]
7. Madhav, S.; Ahamad, A.; Singh, P.; Mishra, P.K. A review of textile industry: Wet processing, environmental impacts, and effluent treatment methods. *Environ. Qual. Manag.* **2018**, *27*, 31–41. [CrossRef]
8. Santos, S.C.; Boaventura, R.A. Adsorption modelling of textile dyes by sepiolite. *Appl. Clay Sci.* **2008**, *42*, 137–145. [CrossRef]
9. Zhu, H.Y.; Fu, Y.Q.; Jiang, R.; Jiang, J.H.; Xiao, L.; Zeng, G.M.; ZHAO, S.L.; Wang, Y. Adsorption removal of congo red onto magnetic cellulose/$Fe_3O_4$/activated carbon composite: Equilibrium, kinetic and thermodynamic studies. *J. Chem. Eng.* **2011**, *173*, 494–502. [CrossRef]
10. Annuar, M.; Adnan, S.; Vikineswary, S.; Chisti, Y. Kinetics and energetics of azo dye decolorization by Pycnoporus sanguineus. *Water Air Soil Pollut.* **2009**, *202*, 79–188. [CrossRef]
11. Saravanan, A.; Kumar, P.S.; Jeevanantham, S.; Karishma, S.; Tajsabreen, B.; Yaashikaa, P.; Reshma, B. Effective water/wastewater treatment methodologies for toxic pollutants removal: Processes and applications towards sustainable development. *Chemosphere* **2021**, *280*, 130595. [CrossRef] [PubMed]
12. Chowdhury, S.; Saha, P. Sea shell powder as a new adsorbent to remove Basic Green 4 (Malachite Green) from aqueous solutions: Equilibrium, kinetic and thermodynamic studies. *Chem. Eng. J.* **2010**, *164*, 168–177. [CrossRef]
13. Albayati, T.M.; Sabri, A.A.; Alazawi, R.A. Separation of methylene blue as pollutant of water by SBA-15 in a fixed-bed column. *Arab. J. Sci. Eng.* **2016**, *41*, 2409–2415. [CrossRef]
14. Saeed, M.; Jamal, M.A.; Haq, A.-U.; Ilyas, M.; Younas, M.; Shahzad, M.A. Oxidative degradation of methylene blue in aqueous medium catalyzed by lab prepared nickel hydroxide. *Int. J. Chem. React. Eng.* **2016**, *14*, 45–51. [CrossRef]
15. Allouche, F.; Yassaa, N. Potential adsorption of methylene blue from aqueous solution using green macroalgae *Posidonia oceanica*. *IOP Conf. Ser. Mater. Sci. Eng.* **2018**, *323*, 012006. [CrossRef]
16. Derakhshan, Z.; Baghapour, M.A.; Ranjbar, M.; Faramarzian, M. Adsorption of methylene blue dye from aqueous solutions by modified pumice stone: Kinetics and equilibrium studies. *Health Scope* **2013**, *2*, 136–144. [CrossRef]
17. Han, T.H.; Khan, M.M.; Kalathil, S.; Lee, J.; Cho, M.H. Simultaneous enhancement of methylene blue degradation and power generation in a microbial fuel cell by gold nanoparticles. *Ind. Eng. Chem. Res.* **2013**, *52*, 8174–8181. [CrossRef]
18. Ali, M.A.; Badawy, A.M.; Seliem, A.Q.; Bendary, H.I.; Lima, E.C.; Al-Dossari, M.; Abd El-Gawaad, N.; Reis, G.S.D.; Mobarak, M.; Hassan, A.M. Macroscopic and microscopic levels of methylene blue adsorption on a magnetic bio-based adsorbent: In-depth study using experiments, advanced modeling, and statistical thermodynamic analysis. *Magnetochemistry* **2024**, *10*, 91. [CrossRef]
19. Pang, Y.; Tong, Z.H.; Tang, L.; Liu, Y.N.; Luo, K. Effect of humic acid on the degradation of methylene blue by peroxymonosulfate. *Open Chem.* **2018**, *16*, 401–406. [CrossRef]
20. Cheng, J.; Zhan, C.; Wu, J.; Cui, Z.; Si, J.; Wang, Q.; Peng, X.; Turng, L.-S. Highly efficient removal of methylene blue dye from an aqueous solution using cellulose acetate nanofibrous membranes modified by polydopamine. *ACS Omega* **2020**, *5*, 5389–5400. [CrossRef]
21. Li, D.; Calebe, V.C.; Li, Y.; Liu, H.; Lei, Y. Interstitial N-Doped $TiO_2$ for Photocatalytic Methylene Blue Degradation under Visible Light Irradiation. *Catalysts* **2024**, *14*, 681. [CrossRef]
22. Sun, L.; Hu, D.; Zhang, Z.; Deng, X. Oxidative degradation of methylene blue via PDS-based advanced oxidation process using natural pyrite. *Int. J. Environ. Res. Public Health* **2019**, *16*, 4773. [CrossRef] [PubMed]
23. Santoso, E.; Ediati, R.; Kusumawati, Y.; Bahruji, H.; Sulistiono, D.; Prasetyoko, D. Review on recent advances of carbon based adsorbent for methylene blue removal from waste water. *Mater. Today Chem.* **2020**, *16*, 100233. [CrossRef]
24. Jawad, A.H.; Abdulhameed, A.S.; Mastuli, M.S. Acid-factionalized biomass material for methylene blue dye removal: A comprehensive adsorption and mechanism study. *J. Taibah Univ. Med. Sci.* **2020**, *14*, 305–313. [CrossRef]
25. Mabel, M.; Sundararaman, T.; Parthasarathy, N.; Rajkumar, J. Chitin Beads from *Peneaus* sp. Shells as a Biosorbent for Methylene Blue Dye Removal. *Pol. J. Environ. Stud.* **2019**, *28*, 2253–2259.

26. Vinita, M.; Dorathi, R.P.J.; Palanivelu, K. Degradation of 2, 4, 6-trichlorophenol by photo Fenton's like method using nano heterogeneous catalytic ferric ion. *Sol. Energy* **2010**, *84*, 1613–1618. [CrossRef]
27. Sayed, M.; Khan, J.A.; Shah, L.A.; Shah, N.S.; Shah, F.; Khan, H.M.; Zhang, P.; Arandiyan, H. Solar light responsive poly (vinyl alcohol)-assisted hydrothermal synthesis of immobilized $TiO_2$/Ti film with the addition of peroxymonosulfate for photocatalytic degradation of ciprofloxacin in aqueous media: A mechanistic approach. *J. Phys. Chem. C* **2018**, *122*, 406–421. [CrossRef]
28. Yang, H.; Li, Y.; Chen, Y.; Ye, G.; Sun, X. Comparison of ciprofloxacin degradation in reclaimed water by UV/chlorine and UV/persulfate advanced oxidation processes. *Water Environ. Res.* **2019**, *91*, 1576–1588. [CrossRef]
29. Iqbal, J.; Shah, N.S.; Khan, J.A.; Naushad, M.; Boczkaj, G.; Jamil, F.; Khan, S.; Li, L.; Murtaza, B.; Han, C. Pharmaceuticals wastewater treatment via different advanced oxidation processes: Reaction mechanism, operational factors, toxicities, and cost evaluation–A review. *Sep. Purif. Technol.* **2024**, *347*, 127458. [CrossRef]
30. Salgado, P.; Márquez, K.; Vidal, G. Vidal Biogenic Synthesis Based on Cuprous Oxide Nanoparticles Using Eucalyptus globulus Extracts and Its Effectiveness for Removal of Recalcitrant Compounds. *Catalysts* **2024**, *14*, 525. [CrossRef]
31. Estrada, A.L.; Li, Y.Y.; Wang, A. Biodegradability enhancement of wastewater containing cefalexin by means of the electro-Fenton oxidation process. *J. Hazard. Mater.* **2012**, *227*, 41–48. [CrossRef] [PubMed]
32. Malato, S.; Fernández-ibáñez, P.; Maldonado, M.I.; Blanco, J.; Gernjak, W. Decontamination and disinfection of water by solar photocatalysis: Recent overview and trends. *Catal. Today* **2009**, *147*, 1–59. [CrossRef]
33. Imoberdorf, G.; Mohseni, M. Kinetic study and modeling of the vacuum-UV photoinduced degradation of 2, 4-D. *Chem. Eng. J.* **2012**, *187*, 114–122. [CrossRef]
34. Khan, J.A.; He, X.; Shah, N.S.; Khan, H.M.; Hapeshi, E.; FAtta-kassinos, D.; Dionysiou, D.D. Kinetic and mechanism investigation on the photochemical degradation of atrazine with activated $H_2O_2$, $S_2O_8^{2-}$ and $HSO_5^-$. *Chem. Eng. J.* **2014**, *252*, 393–403. [CrossRef]
35. Shawaqfeh, A.T.; Al Momani, F.A. Photocatalytic treatment of water soluble pesticide by advanced oxidation technologies using UV light and solar energy. *Sol. Energy* **2010**, *84*, 1157–1165. [CrossRef]
36. Bolton, J.R.; Stefan, M.I. Fundamental photochemical approach to the concepts of fluence (UV dose) and electrical energy efficiency in photochemical degradation reactions. *Res. Chem. Intermed.* **2002**, *28*, 857–870. [CrossRef]
37. Khan, J.A.; He, X.; Khan, H.M.; Shah, N.S.; Dionysiou, D.D. Oxidative degradation of atrazine in aqueous solution by UV/$H_2O_2$/$Fe^{2+}$, UV/$S_2O_8^{2-}$/$Fe^{2+}$ and UV/$HSO_5^-$/$Fe^{2+}$ processes: A comparative study. *Chem. Eng. J.* **2013**, *218*, 376–383. [CrossRef]
38. Hansson, H.; Kaczala, F.; Marques, M.; Hogland, W. Photo-Fenton and Fenton Oxidation of Recalcitrant Wastewater from the Wooden Floor Industry. *Water Environ. Res.* **2015**, *87*, 491–497. [CrossRef]
39. Chen, W.; Zeng, M.; Yang, J. Preparation of Fenton catalysts for water treatment. *Catalysts* **2023**, *13*, 1407. [CrossRef]
40. Hameed, B.; Lee, T. Degradation of malachite green in aqueous solution by Fenton process. *J. Hazard. Mater.* **2009**, *164*, 468–472. [CrossRef]
41. Chen, H.; Bramanti, E.; Longo, I.; Onor, M.; Ferrari, C. Oxidative decomposition of atrazine in water in the presence of hydrogen peroxide using an innovative microwave photochemical reactor. *J. Hazard. Mater.* **2011**, *186*, 1808–1815. [CrossRef] [PubMed]
42. Aleboyeh, A.; Moussa, Y.; Aleboyeh, H. Aleboyeh, The effect of operational parameters on UV/$H_2O_2$ decolourisation of Acid Blue 74. *Dye. Pigment.* **2005**, *66*, 129–134. [CrossRef]
43. Khan, J.A.; Sayed, M.; Shah, N.S.; Khan, S.; Zhang, Y.; Boczkaj, G.; Khan, H.M.; Dionysiou, D.D. Synthesis of eosin modified $TiO_2$ film with co-exposed {001} and {101} facets for photocatalytic degradation of para-aminobenzoic acid and solar $H_2$ production. *Appl. Catal. B Environ.* **2020**, *265*, 118557. [CrossRef]
44. Mehrdad, A.; Massoumi, B.; Hashemzadeh, R. Kinetic study of degradation of Rhodamine B in the presence of hydrogen peroxide and some metal oxide. *Chem. Eng. J.* **2011**, *168*, 1073–1078. [CrossRef]
45. El-Dein, A.M.; Libra, J.; Wiesmann, U. Mechanism and kinetic model for the decolorization of the azo dye Reactive Black 5 by hydrogen peroxide and UV radiation. *Chemosphere* **2003**, *52*, 1069–1077. [CrossRef]
46. Navarro, P.; Zapata, J.P.; Gotor, G.; Gonzalez-olmos, R.; Gómez-lópez, V.M. Degradation of malachite green by a pulsed light/$H_2O_2$ process. *Water Sci. Technol.* **2019**, *79*, 260–269. [CrossRef]
47. Rehman, F.; Sayed, M.; Khan, J.A.; Shah, N.S.; Khan, H.M.; Dionysiou, D.D. Oxidative removal of brilliant green by UV/$S_2O_8^{2-}$, UV/$HSO_5^-$ and UV/$H_2O_2$ processes in aqueous media: A comparative study. *J. Hazard. Mater.* **2018**, *357*, 506–514. [CrossRef]
48. Gao, X.; Guo, Q.; Tang, G.; Peng, W.; Luo, Y.; He, D. Effects of inorganic ions on the photocatalytic degradation of carbamazepine. *J. Water Reuse Desalin.* **2019**, *9*, 301–309. [CrossRef]
49. Yu, X.Y.; Barker, J.R. Hydrogen peroxide photolysis in acidic aqueous solutions containing chloride ions. *I. Chemical mechanism. J. Phys. Chem. A* **2003**, *107*, 1313–1324.
50. Ali, F.; Khan, J.A.; Shah, N.S.; Sayed, M.; Khan, H.M. Carbamazepine degradation by UV and UV-assisted AOPs: Kinetics, mechanism and toxicity investigations. *Process Saf. Environ. Prot.* **2018**, *117*, 307–314. [CrossRef]
51. Malik, P.; Saha, S. Oxidation of direct dyes with hydrogen peroxide using ferrous ion as catalyst. *Sep. Purif. Technol.* **2003**, *31*, 241–250. [CrossRef]
52. Dugandžić, A.M.; Tomašević, A.V.; Radišić, M.M.; Šekuljica, N.Ž.; Mijin, D.Ž.; Petrović, S. Effect of inorganic ions, photosensitisers and scavengers on the photocatalytic degradation of nicosulfuron. *J. Photochem. Photobiol. A* **2017**, *336*, 146–155. [CrossRef]

53. Hoang, N.T.; Mwazighe, F.M. The various effects of hydrogen phosphate and bicarbonate in the degradation of some pollutants in the UV/chlorine and the UV/$H_2O_2$ processes. *J. Water Process Eng.* **2024**, *57*, 104646. [CrossRef]
54. Kan, H.; Soklun, H.; Yang, Z.; Wu, R.; Shen, J.; Qu, G.; Wang, T. Purification of dye wastewater using bicarbonate activated hydrogen peroxide: Reaction process and mechanisms. *Sep. Purif. Technol.* **2020**, *232*, 115974. [CrossRef]
55. Shah, N.S.; Khan, J.A.; Al-muhtaseb, A.A.H.; Sayed, M.; Khan, H.M. Gamma radiolytic decomposition of endosulfan in aerated solution: The role of carbonate radical. *Environ. Sci. Pollut.* **2016**, *23*, 12362–12371. [CrossRef]
56. Merouani, S.; Hamdaoui, O.; Saoudi, F.; Chiha, M.; Pétrier, C. Influence of bicarbonate and carbonate ions on sonochemical degradation of Rhodamine B in aqueous phase. *J. Hazard. Mater.* **2010**, *175*, 593–599. [CrossRef] [PubMed]
57. Aleboyeh, A.; Kasiri, M.B.; Aleboyeh, H. Influence of dyeing auxiliaries on AB74 dye degradation by UV/$H_2O_2$ process. *J. Environ. Manag.* **2012**, *113*, 426–431. [CrossRef]
58. Gogate, P.R.; Pandit, A.B. A review of imperative technologies for wastewater treatment I: Oxidation technologies at ambient conditions. *Adv. Environ. Res.* **2004**, *8*, 501–551. [CrossRef]
59. Yu, X.Y. Critical evaluation of rate constants and equilibrium constants of hydrogen peroxide photolysis in acidic aqueous solutions containing chloride ions. *J. Phys. Chem. Ref. Data* **2004**, *33*, 747–763. [CrossRef]
60. Luna, A.J.; Nascimento, C.A.; Foletto, E.L.; Moraes, J.E.; Chiavone-filho, O. Photo-Fenton degradation of phenol, 2, 4-dichlorophenoxyacetic acid and 2, 4-dichlorophenol mixture in saline solution using a falling-film solar reactor. *Environ. Technol.* **2014**, *35*, 364–371. [CrossRef]
61. Buxton, G.V.; Greenstock, C.L.; Helman, W.P.; Ross, A.B. Critical Review of rate constants for reactions of hydrated electrons, hydrogen atoms and hydroxyl radicals (·OH/·O−) in aqueous solution. *J. Phys. Chem. Ref. Data.* **1988**, *17*, 513–886. [CrossRef]
62. Zhe, Z.; Feng, W.; Nansheng, D. Photochemical reduction of Cr (VI) in aqueous solutions containing Fe (III)-hydroxy complexes. *Toxicol. Environ. Chem.* **2002**, *82*, 129–137. [CrossRef]
63. Tang, W.I.; Huang, C. 2,4-dichlorophenol oxidation kinetics by Fenton's reagent. *Environ. Technol.* **1996**, *17*, 1371–1378. [CrossRef]
64. Sugha, A.; Bhatti, M.S. Degradation of methylene blue dye by UV/$H_2O_2$ advanced oxidation process: Reaction kinetics, residual $H_2O_2$ and specific energy consumption evaluation. *Desalination Water Treat.* **2022**, *274*, 297–307. [CrossRef]
65. Ali, M.A.; Maafa, I.M.; Qudsieh, I.Y. Photodegradation of methylene blue using a UV/$H_2O_2$ irradiation System. *Water* **2024**, *16*, 453. [CrossRef]
66. Banat, F.; Al-Asheh, S.; Nusair, M. Photodegradation of methylene blue dye by the UV/$H_2O_2$ and UV/acetone oxidation processes. *Desalination* **2005**, *181*, 225–232. [CrossRef]
67. Mohammed, H.; Ali, S.K.; Basheer, M. Heavy metal ions removal using advanced oxidation (UV/$H_2O_2$) technique. *IOP Conf. Ser. Mater. Sci. Eng.* **2020**, *870*, 012026. [CrossRef]
68. Jayeola, J.N.; Bello, I.A.; Julius, F.A.; Adio, S.W. Oxidative degradation of methylene blue dye from wastewater by Fenton process. *Int. J. Biol. Sci.* **2022**, *3*, 34–43.
69. Melgoza, D.; Hernández-ramírez, A.; Peralta-hernández, J. Comparative efficiencies of the decolourisation of Methylene Blue using Fenton's and photo-Fenton's reactions. *Photochem. Photobiol. Sci.* **2009**, *8*, 596–599. [CrossRef]
70. Giwa, A.-R.A.; Bello, I.A.; Olabintan, A.B.; Bello, O.S.; Saleh, T.A. Kinetic and thermodynamic studies of Fenton oxidative decolorization of methylene blue. *Heliyon* **2020**, *6*, e04454. [CrossRef]
71. An, T.; An, J.; Gao, Y.; Li, G.; Fang, H.; Song, W. Photocatalytic degradation and mineralization mechanism and toxicity assessment of antivirus drug acyclovir: Experimental and theoretical studies. *Appl. Catal. B Environ.* **2015**, *164*, 279–287. [CrossRef]
72. Huang, G.; Wang, H.; Zhao, H.; Wu, P.; Yan, Q. Application of polypyrrole modified cathode in bio-electro-Fenton coupled with microbial desalination cell (MDC) for enhanced degradation of methylene blue. *J. Power Sources* **2018**, *400*, 350–359. [CrossRef]
73. Wang, Q.; Tian, S.; Ning, P. Degradation mechanism of methylene blue in a heterogeneous Fenton-like reaction catalyzed by ferrocene. *Ind. Eng. Chem. Res.* **2014**, *53*, 643–649. [CrossRef]
74. Huang, F.; Chen, L.; Wang, H.; Yan, Z. Analysis of the degradation mechanism of methylene blue by atmospheric pressure dielectric barrier discharge plasma. *Chem. Eng. J.* **2010**, *162*, 250–256. [CrossRef]
75. Yu, X.; Zhang, J.; Chen, Y.; Ji, Q.; Wei, Y.; Niu, J.; Yu, Z.; Yao, B. Ag-$Cu_2O$ composite films with enhanced photocatalytic activities for methylene blue degradation: Analysis of the mechanism and the degradation pathways. *J. Environ. Chem. Eng.* **2021**, *9*, 106161. [CrossRef]
76. Wang, H.; Wang, H.; Yan, Q. Peroxymonosulfate activation by algal carbocatalyst for organic dye oxidation: Insights into experimental and theoretical. *Sci. Total Environ.* **2022**, *816*, 151611. [CrossRef]
77. Khan, J.A.; Sayed, M.; Shah, N.S.; Khan, S.; Khan, A.A.; Sultan, M.; Tighezza, A.M.; Iqbal, J.; Boczkaj, G. Synthesis of N-doped $TiO_2$ nanoparticles with enhanced photocatalytic activity for 2, 4-dichlorophenol degradation and $H_2$ production. *J. Environ. Chem. Eng.* **2023**, *11*, 111308. [CrossRef]
78. ECOSAR. 2022. Available online: https://www.epa.gov/tsca-screening-tools/ecological-structure-activity-relationships-ecosar-predictive-model (accessed on 10 November 2024).

79. Wang, S.; Zhou, N. Removal of carbamazepine from aqueous solution using sono-activated persulfate process. *Ultrason Sonochem.* **2016**, *29*, 156–162. [CrossRef]
80. De Luca, A.; De Benedetto, A.; Cascione, M.; De Matteis, V.; Di Corato, R.; Corrado, M.; Rinaldi, R. Eco-friendly $TiO_2$ nanoparticles: Harnessing Aloe vera for superior photocatalytic degradation of methylene blue. *Catalysts* **2024**, *14*, 820. [CrossRef]